PHILOSOPHICAL TRANSACTIONS A

rsta.royalsocietypublishing.org

Research

Cite this article: Greco M, Lugni C, Faltinsen OM. 2015 Influence of motion coupling and nonlinear effects on parametric roll for a floating production storage and offloading platform. *Phil. Trans. R. Soc. A* **373**: 20140110. http://dx.doi.org/10.1098/rsta.2014.0110

One contribution of 12 to a Theme Issue 'Advances in fluid mechanics for offshore engineering: a modelling perspective'.

Subject Areas:
ocean engineering, mechanical engineering, fluid mechanics

Keywords:
parametric roll, motion coupling, three-dimensional domain-decomposition, stability analysis

Author for correspondence:
C. Lugni
e-mail: claudio.lugni@cnr.it

Electronic supplementary material is available at http://dx.doi.org/10.1098/rsta.2014.0110 or via http://rsta.royalsocietypublishing.org.

Influence of motion coupling and nonlinear effects on parametric roll for a floating production storage and offloading platform

M. Greco[1,2], C. Lugni[1,2] and O. M. Faltinsen[2]

[1]CNR-INSEAN, The Italian Ship Model Basin, via di Vallerano 139, 00128 Rome, Italy
[2]Centre for Autonomous Marine Operations and Systems (AMOS), Department of Marine Technology, NTNU, Trondheim, Norway

Occurrence and features of parametric roll (PR) on a weather-vaning floating production storage and offloading (FPSO) platform with a turret single-point mooring-line system are examined. The main focus is on the relevance of motions coupling and nonlinear effects on this phenomenon and on more general unstable conditions as well as on the occurrence and severity of water on deck. This work was motivated by recent experiments on an FPSO model without mooring systems highlighting the occurrence of parametric resonance owing to roll–yaw coupling. A three-dimensional numerical hybrid potential-flow seakeeping solver was able to capture this behaviour. The same method, extended to include the mooring lines, is adopted here to investigate the platform behaviour for different incident wavelengths, steepnesses, headings, locations of the turret and pre-tensions. From the results, sway and yaw tend to destabilize the system, also bringing chaotic features. The sway–roll–yaw coupling widens the existence region of PR resonance and increases PR severity; it also results in a larger amount of shipped water, especially at smaller wavelength-to-ship length ratio and larger steepness. The chaotic features are excited when a sufficiently large yaw amplitude is reached. Consistently, a simplified stability analysis showed the relevance of nonlinear-restoring coefficients, first those connected with the sway–yaw coupling then those associated with the roll–yaw coupling, both destabilizing. From the stability analysis, the system is

THE ROYAL SOCIETY PUBLISHING

unstable for all longitudinal locations of the turret and pre-tensions examined, but the instability weakens as the turret is moved forward, and the pre-tension is increased. The use of a suitable dynamic-positioning system can control the horizontal motions, avoiding the instability.

1. Introduction

Parametric roll (PR) is a resonance and instability phenomenon which can influence different vessels, for example, from fishing to cruise vessels to container vessels. The first investigations on this subject examined its occurrence in following seas (see e.g. review in reference [1]), while more recently attention has been focused on head-sea conditions confirmed as an important destabilizing mechanism (see e.g. review in reference [2]). PR is recognized to be induced by changes in the transverse metacentric height (GM) and so in the restoring properties of the vessel caused by the interaction with incident waves and by sufficiently large heave and pitch motions. From [3], its occurrence is supported by incident waves that do not change much in amplitude and period, that tend to be aligned to the vessel longitudinal axis and are associated with a natural roll frequency-to-incident wave frequency ratio $\omega_{4n}/\omega = 0.5$, 1, 2 and so on. This means that head-sea regular waves with proper period T are the best candidates to cause PR; despite this, such a phenomenon is not recognized as an issue for weather-vaning floating production storage and offloading (FPSO) platforms which are moored without or with dynamic-positioning (DP) support. However, water-on-deck (WOD) experiments in reference [4] on an FPSO without a station-keeping system documented roll instability both owing to interaction with incident waves and large heave and pitch motions, and owing to a yaw–roll unstable coupling. The latter phenomenon motivated the present numerical research activity. A method for violent wave–body interactions, detailed in reference [5] and validated against experiments involving WOD, bottom-slamming and PR events, has been extended to include mooring-line loads using a nonlinear quasi-static approach and applied to investigate occurrence of PR and of more general instability phenomena on a weather-vaning moored FPSO. The focus is on the influence of motions coupling and nonlinear effects.

In §2, the adopted numerical solver is described; then in §3 the experimental case with PR induced by yaw–roll coupling is discussed because it represents the motivation and background for this work. Current physical investigation is documented in §4, and then the major conclusions are drawn.

2. Numerical solver

The station-keeping problem of an FPSO platform is modelled numerically with a three-dimensional hybrid solver based on a domain-decomposition (DD) strategy. The basic DD involves three methods (A, B and C) and is described comprehensively in reference [5], whereas here the major features are provided, and more emphasis is given to the method extension to account for the mooring-line loads.

(a) Original numerical strategy

The basic DD couples a global external method (A) handling the wave–body interaction and an in-deck shallow-water approximation (B) applicable for dam-break and large-scale evolution of plunging-wave *plus* dam-break types of water shipping, the latter identified as the most common WOD scenario [6]. Method B simulates the water shipping phenomenon on a two-dimensional Cartesian grid fixed to the deck and transforming the related problem into a sequence of one-dimensional coupled problems along the main axes of the computational grid. In each direction, the fluxes of the flow variables are estimated by an exact Riemann solver, and the coupled

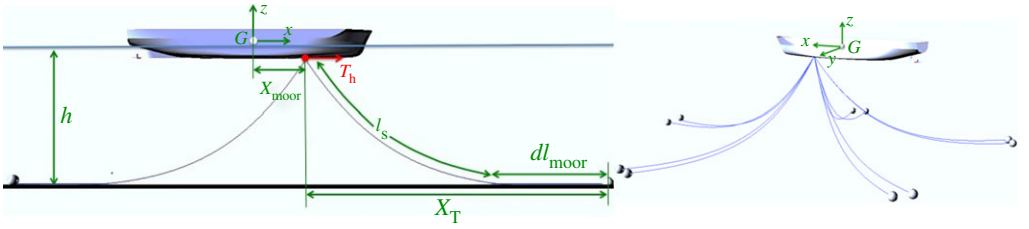

Figure 1. Mooring-line system. (*a*) Definition of cable parameters in the cable plane here incidentally coincident with the *x*–*z*-plane. (*b*) Sketch of a generic cable arrangement. (Online version in colour.)

equations are stepped forward in time with a first-order scheme. In general, the deck profile and possible superstructures are immersed on the grid, so the level-set technique in reference [7] is adopted to suitably enforce the related boundary conditions. A local bottom-slamming solution (C) based on a Wagner-type [8] approach is also modelled to handle slamming during the water-entry phase of the ship. The B and C methods receive local information from solver A, the former in terms of water level and velocity distributions along the deck profile and motion conditions of the deck, and the latter in terms of relative motion and velocity at the ship bottom. In return, they provide the loads connected with the WOD and bottom-slamming phenomena, respectively. These loads are inserted in the platform-motion equations, formulated in the time domain, that can be integrated in time so as to prolong the instantaneous ship configuration provided by method A. This global wave–ship interaction solver is based on the weak-scatterer hypothesis [9], assuming that incident waves and body motions are large relative to the scattering and radiation effects. It implies that theoretically this approximation is valid for wavelength-to-ship length ratios sufficiently large. Consistently, with this assumption, the impermeability body-boundary condition is enforced to be satisfied averagely along the instantaneous wetted hull surface defined by the incident waves and the body motions, which leads to a correction of the scattering and radiation loads obtained from linear theory. Moreover, nonlinearities are retained up to the second order for Froude–Krylov and hydrostatic loads.

The solver has been successfully validated against WOD and PR experiments on the FPSO platform examined in the next section [10]. Moreover, the method provided satisfactory results against WOD model tests and compared fairly well with added-resistance measurements on a patrol ship [11].

(b) Extension of the solver to handle mooring-line loads

In addition to the described features, here a fourth method is included for the estimation of the anchorline loads acting on a moored ship. The mooring-line system is modelled as a set of N_c steel inelastic anchor-lines with weight per unit length in water equal to w_c, attached to the ship through a turret at $\boldsymbol{X}_{\mathrm{moor}}$ and radially distributed. All cables have the same pre-tension T_0, and the same total length $L_{\mathrm{T}} = l_{\mathrm{s}} + dl_{\mathrm{moor}}$, with l_{s} the length of the suspended part in a sea region with water depth h and with dl_{moor} the length of the portion laying on the sea floor. The cable projection in the horizontal plane is X_{T}, and the horizontal tension acting at the contact point with the vessel is T_{h}. Variable definitions and the generic arrangement of the cables are provided in figure 1. The initial values of l_{s} and dl_{moor}, i.e. $l_{\mathrm{s}}0$ and $dl_{\mathrm{moor}}0$, are assumed the same for each cable and found enforcing equilibrium conditions in calm water under the pre-tension action (the needed relationships can be found, e.g. in reference [12]). The values in time of l_{s} and dl_{moor} differ, in general, instead, from cable to cable, owing to the interactions with the environment, with the constraint that their sum L_{T} remains constant for each anchorline. Taking a single cable, the changes in its configuration are induced by the platform horizontal motions. These lead to a displacement of the cable contact point with the ship. The projection of this horizontal displacement in the cable plane, say dx_{moor}, results in a change of X_{T} from its

original value X_T0, as $X_T = X_T0 + dx_{moor}$, and leads, in general, to a variation of l_s and dl_{moor}. The horizontal tension induced by each cable on the vessel as a consequence of the action and reaction principle is obtained assuming valid a quasi-static approach but retaining a nonlinear cable description. In particular, the approach indicated as method 2 in reference [13] is followed, which involves the nonlinear constraint

$$\cosh\left[\sqrt{\left(\frac{w_c h}{T_h}\right)^2 + 2\frac{w_c h}{T_h}} - \frac{w_c(L_T - X_T)}{T_h}\right] - \frac{w_c h}{T_h} - 1 = 0. \tag{2.1}$$

This relationship is obtained combining geometric and tension links for the equilibrium of a deep-sea catenary and needs an iterative process to be satisfied. In the present case, a Newton–Raphson method is used. More in detail, at any time instant solver A provides the actual position of the cable contact point, i.e. $\boldsymbol{X}_{moor}$, which is used as input for the mooring-line problem to estimate the instantaneous value of X_T needed in equation (2.1). This allows to find iteratively the actual horizontal tension acting on each cable at the contact point with the ship which ensures the equilibrium of the mooring-line and preserves the value of the total cable length L_T. Once known $T_{h,i}$ provided by each cable i, as well as the instantaneous configuration of the cables, the surge and sway force and the yaw moment induced by the whole mooring system on the ship can be estimated at the examined time instant and introduced in the body-motion equations.

(c) Resulting numerical solver

The equations of motions are solved in time domain using the approach in reference [14]. This is necessary to simulate the transient phase of the motions. The resulting strategy involves convolution integrals to express the radiation loads and strictly speaking is valid for linear wave–body interactions. However, it is also applied, in practice, to include nonlinear loads when the radiation loads are still assumed linear. In the present case, radiation and scattering effects are both assumed small, moreover, they are combined through the instantaneous enforcement of the body-boundary condition, described more in detail below in the text, so their corresponding loads cannot be separated and are expressed by means of convolution integrals.

The rigid-body motion equations are written along a body-fixed coordinate system with origin in the centre of gravity and read

$$\begin{aligned} \boldsymbol{M}\ddot{\boldsymbol{\xi}} + \boldsymbol{\Omega} \times \boldsymbol{M}\dot{\boldsymbol{\xi}} + \boldsymbol{A}_\infty\dot{\boldsymbol{\beta}} + \int_0^t \boldsymbol{K}(t-\tau)\dot{\boldsymbol{\beta}}(\tau)\,\mathrm{d}\tau \\ = \boldsymbol{F}_{0\,\mathrm{nlin}} + \boldsymbol{F}_{h\,\mathrm{nlin}} + \boldsymbol{F}_{\mathrm{wod}} + \boldsymbol{F}_{\mathrm{slam}} + \boldsymbol{F}_{\mathrm{moor}} \end{aligned} \tag{2.2}$$

with $\boldsymbol{M}$ the ship generalized mass matrix, $\boldsymbol{\xi} \equiv (\xi_1, \ldots, \xi_6)$ the six rigid degrees of freedom (6 d.f.), $\boldsymbol{\Omega}$ the angular velocity vector $(\dot{\xi}_4, \dot{\xi}_5, \dot{\xi}_6)$ and the upper dots indicating time (t) derivatives performed along the instantaneous body axes. In equation (2.2), the six-component vector associated with the cross product is obtained through the cross-product of $\boldsymbol{\Omega}$ with the first three components of $\boldsymbol{M}\dot{\boldsymbol{\xi}}$, whereas the remaining components are given by the cross-product of $\boldsymbol{\Omega}$ with the second three components of $\boldsymbol{M}\dot{\boldsymbol{\xi}}$. $\boldsymbol{A}_\infty$ is the infinite-frequency added-mass matrix and $\boldsymbol{K}$ is the retardation-function matrix. Nonlinear effects are included in the right-hand side in the Froude–Krylov, $\boldsymbol{F}_{0\,\mathrm{nlin}}$, hydrostatic, $\boldsymbol{F}_{h\,\mathrm{nlin}}$, slamming, $\boldsymbol{F}_{\mathrm{slam}}$, WOD, $\boldsymbol{F}_{\mathrm{wod}}$ and mooring-line, $\boldsymbol{F}_{\mathrm{moor}}$, loads. A correction is also present in the added-mass and convolution-integral terms in left-hand side of equation (2.2). This is due to the presence of $\boldsymbol{\beta}(\tau)$ which substitutes $\dot{\boldsymbol{\xi}}$ appearing in the linear equations of motion. $\boldsymbol{\beta}(\tau)$ is connected with the weak-scatterer assumption and is estimated in time from the body-boundary condition

$$V_n(\boldsymbol{x}, t) = (\boldsymbol{V}_{\mathrm{ship}} - \boldsymbol{V}_{\mathrm{wave}}) \cdot \boldsymbol{n} \tag{2.3}$$

enforced on the instantaneous wetted-surface of the ship defined by the incident waves and the body motions. Here, V_n is the fluid-velocity component along the hull normal vector $\boldsymbol{n}$, $\boldsymbol{V}_{\mathrm{ship}}$ is the body velocity and $\boldsymbol{V}_{\mathrm{wave}}$ is the incoming-wave velocity. This implies that radiation and scattering

phenomena are considered together, as mentioned earlier in the text. To enforce condition (2.3), V_n is expressed in terms of N prescribed basis functions ψ_i,

$$V_n(\boldsymbol{x}, t) = \sum_{i=1}^{i=N} \beta_i(t)\psi_i(\boldsymbol{x}), \tag{2.4}$$

with β_i the ith component of $\boldsymbol{\beta}$, and the resulting condition (2.3) is enforced through a minimum least-square approach along the wetted hull. This provides the equations to find $\boldsymbol{\beta}$. Here, $N = 6$ with $\psi_i = n_i$ are adopted, n_i being the ith component of the generalized normal vector to the ship. In this way, the retardation function matrix $\boldsymbol{K}$ can be obtained from either the added-mass or the damping coefficients estimated from the usual linear radiation problems.

The obtained equations of motions are solved numerically in time using a fourth-order Runge–Kutta scheme. When evolving from time t to $t + \Delta t$, the WOD loads, the slamming loads, the convolution integral terms and the mooring-line loads are estimated in t and retained constant during the time interval Δt. The other loads are estimated at any time instant required by the scheme. The convolution integrals are evaluated by using a step-wise linear interpolation of $\boldsymbol{K}(t - \tau)$ and $\boldsymbol{\beta}(\tau)$ components and then integrating analytically from $\tau^* < t$ to t with τ^* chosen so that for times less than τ^* the memory effects, and so the components of the retardation-function matrix, are negligible.

The adopted DD strategy can estimate only the wave-radiation potential-flow damping. Viscous roll damping from the hull is obtained from the free-decay tests performed as preliminary step of the experiments described in §3 and modelled as a linear damping in the simulations. In this way it is assumed that the damping is not affected much by the change of the natural frequency caused by motions coupling. This might be questionable; however, a better estimation would require tests with forced oscillation motions which are not straightforward. The mooring-line damping for surge, sway and yaw are assumed as second-order loads with damping coefficients equal to the 10% of the corresponding critical damping. One must note that the damping loads for a given system depend on wave frequency and amplitude and on mean line tension, here this damping level is chosen arbitrarily but consistently with documented order of magnitude of the mooring-line damping [15]. The influence of this parameter is left for future investigations.

3. Motivation: influence of roll–yaw coupling during FPSO experiments

Three-dimensional model tests were performed at basin no. 2 (length × width × depth = 220 × 9 × 3.6 m) of CNR-INSEAN on an FPSO ship in scale 1 : 40 without bilge-keels and mooring-line system. They aimed to examine WOD and PR occurrence and features. The experimental set-up was designed to restrain surge, sway and yaw by means of a gimble placed in the hull and combined with a vertical shaft. The latter slides in a bearing blocked in the horizontal plane. The gimble allows the roll and pitch motions, whereas the vertical shaft leaves free the heave. Because of the cylindrical shape of the shaft, the yaw motion should be restrained through a load cell. In reality, during the tests, the vessel experienced yaw motion owing to problems in the arrangement, as it is discussed later in the text.

The ship body plan and the main hydrostatic properties are provided in figure 2. The roll natural period in calm water and the roll damping were estimated through free-decay tests giving a calm-water 1-d.f. roll natural period $T_{4n0} = 2\pi/\omega_{4n0} \simeq 3.56$ s and an approximated linear-damping coefficient $B_{44,1} \simeq 0.0262 B_{44}^{\text{crit}}$, with B_{44}^{crit} the critical damping. This damping is relatively small for practical FPSOs because it does not include for instance the bilge keels and mooring-line effects.

The incident waves were generated as regular systems with heading angle of 180 (head-sea), 175 and 170 degrees, steepness kA between 0.1 and 0.25 with step 0.05, and wavelength-to-ship length ratios $\lambda/L = 0.75$, 1, 1.25, 1.5 and 2, which are relevant for water-shipping occurrence. This λ/L range corresponds to the calm-water roll natural frequency-to-excitation frequency ratio,

(a)

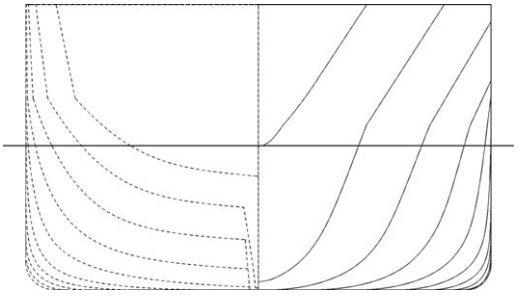

(b)

length (L)	scale 1 : 40	4.22 m
breadth (B)		0.8l m
draft (D)		0.25 m
displacement		663 kg
metacentric height (GM)		0.036 m
pitch gyration radius (K_{yy})		0.27 L
roll gyration radius (K_{xx})		0.37 B

Figure 2. Experimental set-up: (*a*) FPSO body plan and (*b*) main hydrostatic properties.

ω_{4n0}/ω, within [0.402,0.656] and so to incident-wave conditions in the region of first parametric resonance for the roll, which occurs at $\omega_{4n}/\omega = 0.5$ with ω_{4n} the actual value of the roll natural frequency. This value can be modified in waves by coupling with other motions and nonlinear effects. As a result, the experiments allowed to investigate WOD and PR phenomena and their mutual influence.

Different local and integrated quantities were monitored during the tests, particularly the rigid ship motions and the evolution of the wave–body interaction through video recordings. A detailed description of the model tests and related errors are documented in [11], and in [10] the physical studies of interest for the present investigations are examined.

The in-depth analysis of the cases with heading angle $\beta = 175^\circ$ complemented by numerical simulations performed with the basic solver described in §2, highlighted a relevant effect of roll–yaw coupling in the occurrence of roll resonance with consequences also for the WOD severity. Preliminary results are documented in reference [4]. Here, the major outcomes, motivating the present analysis, are summarized. For $\beta = 175^\circ$ and $\omega_{4n0}/\omega > 0.464$, PR phenomena were recorded at sufficiently large steepnesses, whereas in head-sea conditions, nonlinear effects tend to avoid the instability at those frequency ratios. The reason for this different behaviour was found examining the case with $\omega_{4n0}/\omega = 0.519$ and $kA = 0.25$ that experienced an accident and was repeated. Consistently, with the numerical simulations, the first run (run 44, see the electronic supplementary material, movie S1) was not associated with PR and produced a large amount of WOD (figure 3*a*) partially leaking inside the ship model and so leading to a drift in time of heave and pitch motions. The vessel was then made waterproof and the test repeated as run 46 (see the electronic supplementary material, movie S2) experiencing PR and also WOD but without leakage (figure 3*b*). Because, for runs 44 and 46, the prescribed incident waves are the same, but the resulting ship behaviour is different, these tests were examined more in detail so as to identify the mechanism exciting the PR in run 46. From the three-dimensional videos, the shaft used to block the yaw experienced a slack worsened by the accident during run 44 and affecting the ship's behaviour especially in long and severe waves. The evolutions of the yaw motion for run 44 and 46 are compared in figure 3*c* and confirm a quite limited but non-zero amplitude for the former case, indicating that the shaft had a slack even before the accident but was more limited. Run 46, experiencing much larger yaw, was then used to investigate the connection between roll–yaw coupling and PR occurrence. Figure 4 documents the phase plots for roll and yaw motions related to the four parts of the motion evolution indicated in figure 3*c*. At the beginning (first part), linear effects dominate and both motions oscillate with the incident-wave period; then (second part), ξ_6 becomes chaotic and the coupling with ξ_4 leads to a smaller roll natural period, in particular changing from $2T$ (first PR resonance) to $1.5T$. In the third phase (third part), the yaw becomes regular with main period $3T$ and the roll is dominated by the period $1.5T$ and modulated by the yaw period $3T$, leading to two modes in the roll phase plot. In the last part, the yaw motion is again chaotic, and nonlinear effects dominate the yaw–roll coupling.

The relevance of the yaw–roll coupling for the instability was confirmed by the DD simulations with the hydrodynamic coefficients connected with the yaw and its coupling with roll included in

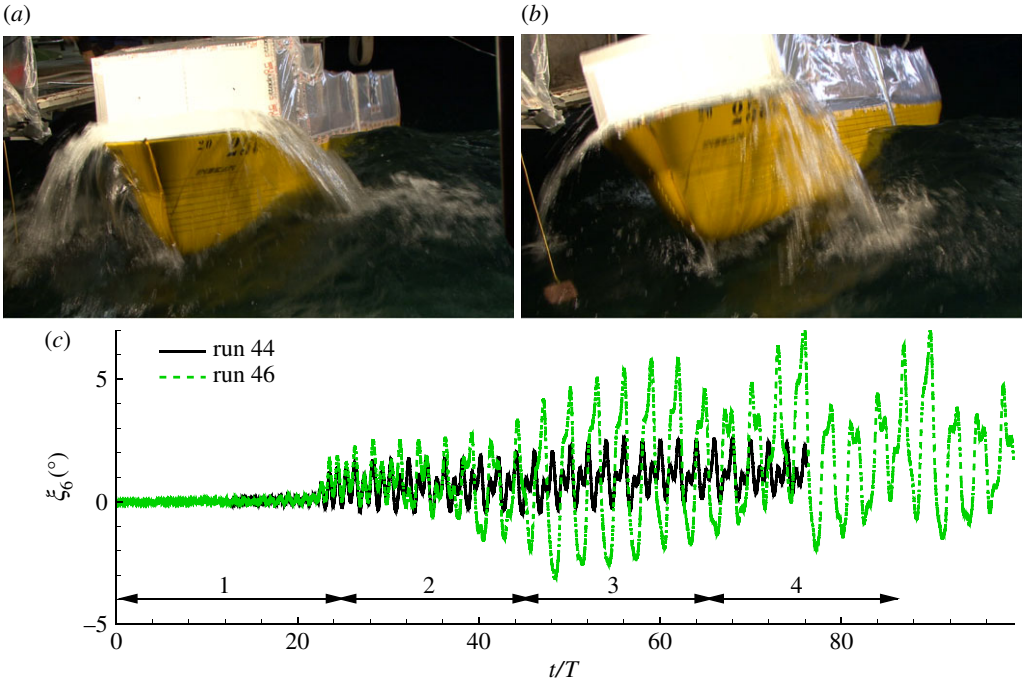

Figure 3. Incident waves with $\omega_{4n0}/\omega = 0.519$ and $kA = 0.25$. Run 44 (*a*; see electronic supplementary material, movie S1) and run 46 (*b*; see electronic supplementary material, movie S2) at the time instant with wave crest at mid-ship. (*c*) Yaw motion for the two runs. (Online version in colour.)

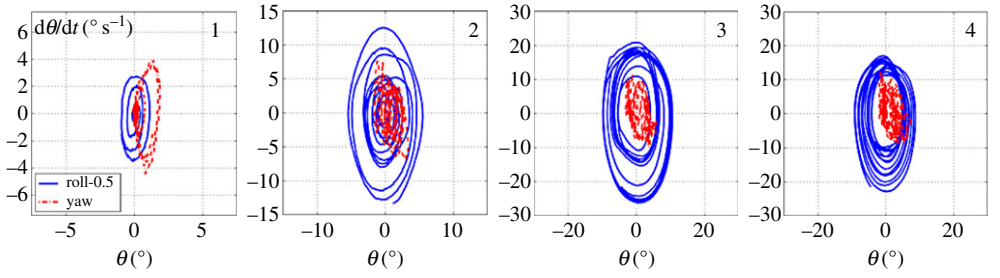

Figure 4. Incident waves with $\omega_{4n0}/\omega = 0.519$ and $kA = 0.25$: run 46. Phase plots associated with the four stages of the roll and yaw motions evolutions indicated in figure 3*c*. Here, θ indicates ξ_4 (solid lines) or ξ_6 (dashed lines). (Online version in colour.)

the motions equations. Such coefficients were estimated using the available load measurements and assuming a 2-d.f. yaw–roll coupled system. The heave, pitch, roll and yaw motions from the simulations are compared in figure 5 with the corresponding predictions assuming zero yaw and with the time histories measured for run 46 during the third phase of the evolution discussed above, i.e. the one where the yaw is dominated by the period $3T$ and the roll by the period $1.5T$. ξ_3 and ξ_5 are not much affected by the yaw inclusion, whereas the roll motion confirms the occurrence of PR as in the experiments. The yaw amplitudes are not fully captured by the method, because of the simplifications in the identification process of the hydrodynamic coefficients connected with ξ_6.

In this example, the restoring and damping connected with the yaw are rather large since they are associated with the slack of the shaft, whereas in the practical conditions of a moored weather-vaning FPSO, they will be connected with the mooring-line systems and therefore much more limited. Greater damping can be obtained through combining the cables with

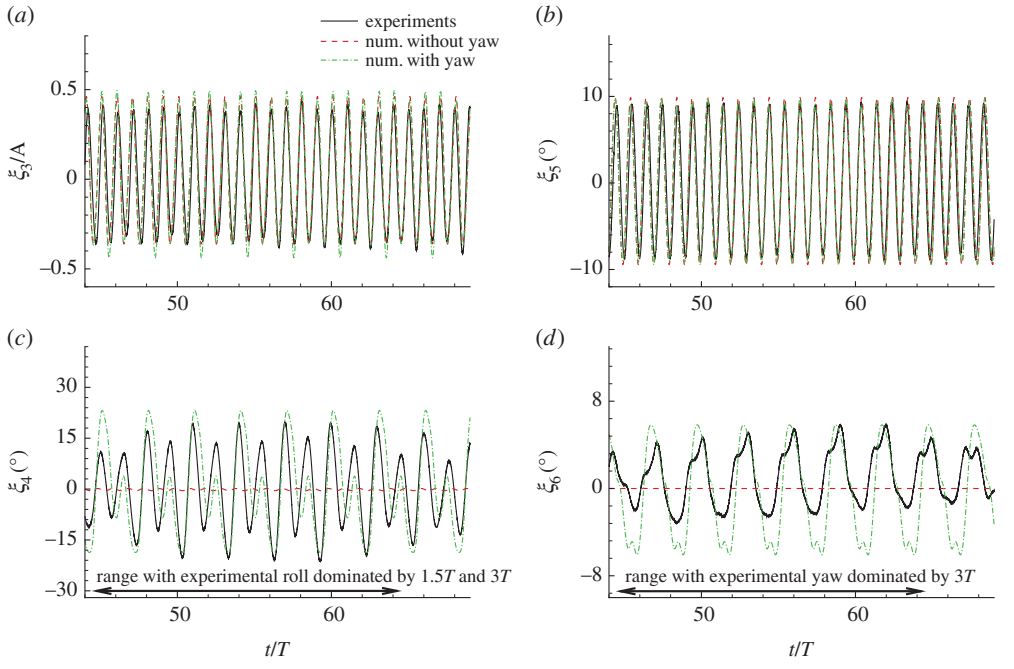

Figure 5. Incident waves with $\omega_{4n0}/\omega = 0.519$ and $kA = 0.25$: heave (*a*), pitch (*b*), roll (*c*) and yaw (*d*) experimental motions for run 46 and those obtained numerically by the DD solver without and with yaw motion. (Online version in colour.)

a dynamic-positioning system. These conditions are examined in §4 using the described experiments as framework in terms of ship geometry and wave conditions and therefore bilge keels and other roll-damping devices are not accounted for. Moreover, in these experiments, the sway was restrained, whereas the numerical analysis will consider also the importance of this motion and its coupling with roll and yaw.

4. Physical investigations

The FPSO platform examined in the model tests discussed above is assumed to be weather-vaning thanks to a single-point turret system with $\boldsymbol{X}_{\mathrm{moor}} = (X_{\mathrm{moor}} = 0.25L, 0, 0)$ and made of $N_c = 10$ anchorlines arranged radially at $72 \times i \pm 2.5$ degrees ($i = 0, 1, 2, 3, 4$) from the platform longitudinal axis x (see the sketch in figure 6). The weight per unit length is assumed $w_c = 1884\,\mathrm{N\,m^{-1}}$, the water depth h is taken as 200 m, the pre-tension $T_0 = 2000\,\mathrm{kN}$ and $dl_{\mathrm{moor}}0$ is set as $l_{\mathrm{min,moor}} - l_s0$, with $l_{\mathrm{min,moor}} = h\sqrt{2T_{\mathrm{break}}/(hw_c) - 1}$ (e.g. [12]) and the cable break load $T_{\mathrm{break}} = 12\,000\,\mathrm{kN}$. It is also assumed that the anchorlines provide a second-order damping for surge, sway and yaw with damping coefficients equal to the 10% of the corresponding critical damping. The parameters were set equal to typical values for similar FPSOs in similar operating conditions (Skjørdal 2014, personal communication).

To assess the effect of the mooring-line system, the regular head-sea conditions tested experimentally and numerically with fixed surge, sway and yaw, were examined. Unless explicitly stated, present numerical simulations were performed until $t = 400T$ using a time step $\Delta t = 0.005T$, with T the incident-wave period.

(a) Parametric-roll and water-on-deck phenomena

The comparisons among the different results are documented in table 1 in terms of PR and WOD occurrences. The station-keeping system has a limited influence on water-on-deck occurrence and also the green-water severity is not much affected but for the largest steepness cases, as

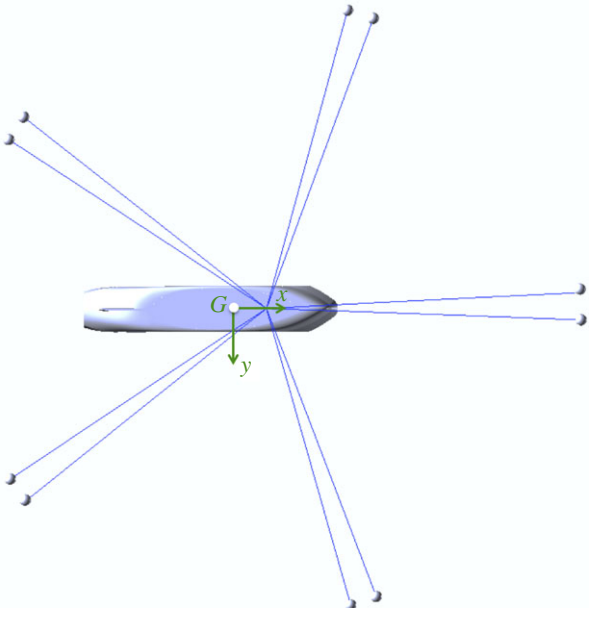

Figure 6. Mooring-line system: cable arrangement used for the investigation. (Online version in colour.)

documented by the maximum amount of shipped water provided in the plot of figure 7*a*. The anchorlines clearly widen instead the region of PR instability around $\omega_{4n0}/\omega = 0.464$ when the incident-wave steepness is large enough. They also affect the amplitudes of the PR excited even without cables, as confirmed by plot of figure 7*b*. In all cases, the PR severity is increased, especially at $\omega_{4n0}/\omega = 0.464$. In some cases, the angles reached are very large owing to the coupling with large horizontal motions. This suggests the need of a DP system to complement the damping from the mooring-lines, because thrusters can provide linear damping up to the 60% of the critical damping.

(b) Instability phenomena and chaotic behaviour

The additional PR phenomena connected with the moored FPSO are induced by the coupling among different degrees of freedom leading to system instability whose occurrence is examined in table 2. From the results, except for the lowest steepnesses, there is a clear unstable behaviour of the system. In some severe conditions, the instability leads to the breakdown of the numerical solution owing to very large motion amplitudes and so to critical configurations of the platform. The existence domain of the motion instability is wider than that of the PR identified by a roll natural period near the first-parametric resonance. Moreover, the instability will always lead to chaotic features of the motions within a time interval that depends on the involved nonlinearities. This has been checked for $\omega_{4n0}/\omega = 0.464$. With $kA = 0.15$, the chaotic behaviour is excited at about $200T$, with $kA = 0.1$ and with a smaller steepness $kA = 0.05$ the simulation time was prolonged after $400T$ and showed the chaotic features around $440T$ for $kA = 0.1$ and at about $2300T$ for $kA = 0.05$. The reason for the different time intervals required for the chaotic excitation is suggested by the motion time histories. In particular, the case with $\omega_{4n0}/\omega = 0.464$ and $kA = 0.15$ is taken as an example to show the typical features of surge, sway, roll and yaw evolutions when instability with chaotic development occurs (figure 8). First, the motions grow as for the usual diverging systems; this instability trend is especially evident for the yaw. Then, it seems that, once ξ_6 has reached a certain threshold value (in this case slightly before $200T$), the system becomes chaotic and quite large amplitudes are observed for all horizontal motions coming into the irregular regime. The mooring-line system leads to small restoring and so to large natural periods for the horizontal

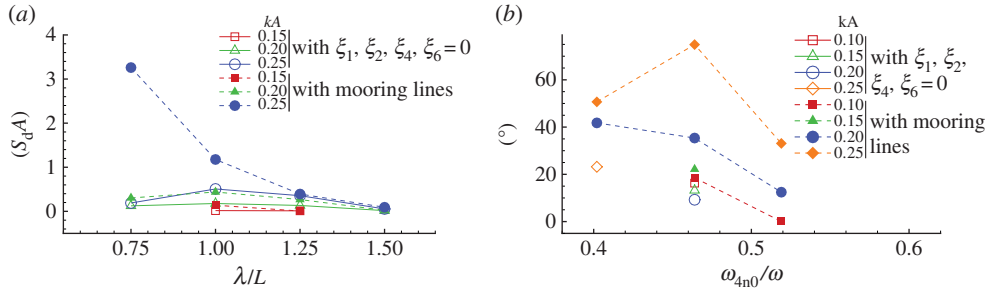

Figure 7. Influence of mooring-line system on water on deck and PR from numerical analysis at large times, i.e. $t > 300T$. (*a*) Maximum volume of shipped water Q. Q is made non-dimensional by S_dA, with S_d the deck area and A the incident-wave amplitude, and is plotted for each examined steepness kA as a function of the ratio between the incident wavelength and the ship length, λ/L. (*b*) Amplitude of PR as a function of kA and of the calm-water roll natural frequency-to-excitation frequency ratio, ω_{4n0}/ω. (Online version in colour.)

Table 1. Occurrence of water on deck (WOD, left) and parametric-roll resonance (PR, right) for the cases studied experimentally and reproduced numerically in head-sea conditions, i.e. $\beta = 180$. For PR: NI = with very weak unstable behaviour; for WOD: NI = very small amount of shipped water, in the numerical case this corresponds to a full-scale mean water level on the deck less than 8 cm and yes* = WOD caused by PR. X = cases not performed experimentally and so neither numerically.

$\lambda/L \rightarrow$	0.75	1.00	1.25	1.50	2.00	0.75	1.00	1.25	1.50	2.00
$\omega_{4n0}/\omega \rightarrow$	0.402	0.464	0.519	0.568	0.656	0.402	0.464	0.519	0.568	0.656
method kA	WOD					PR				
exper. 0.10	no	no	no	no	no	no	yes	no	no	no
num 0.10	no	no	no	no	no	no	yes	no	no	no
num moor 0.10	no	no	no	no	no	no	yes	NI	no	no
exper. 0.15	no	no	NI	no	no	no	yes	no	no	no
num 0.15	no	NI	NI	no	no	no	yes	no	no	no
num moor 0.15	no	yes	NI	no	no	no	yes	no	no	no
exper. 0.20	yes*	yes	yes	yes	X	yes	no	no	no	X
num 0.20	yes*	yes	yes	yes	X	yes	yes	no	no	X
num moor 0.20	yes*	yes	yes	yes	X	yes	yes	yes	no	X
exper. 0.25	yes	yes	yes	yes	X	yes	no	no	no	X
num 0.25	yes	yes	yes	yes	X	yes	no	no	no	X
num moor 0.25	yes	yes	yes	yes	X	yes	yes	yes	no	X

motions (i.e. roughly 67, 85 and 80 s for surge, sway and yaw motions, respectively, using the restoring provided by the cables in their initial configuration). Consequently, the sway–roll–yaw coupling is not able to modify the roll natural period when PR occurs, as instead documented by the experiments with slacked shaft (see §3). However, the roll is subjected to an irregular envelope connected with the chaotic change of the sway and yaw oscillation periods. Then, ξ_4 experiences a sort of weaker chaotic behaviour, only associated with the amplitude.

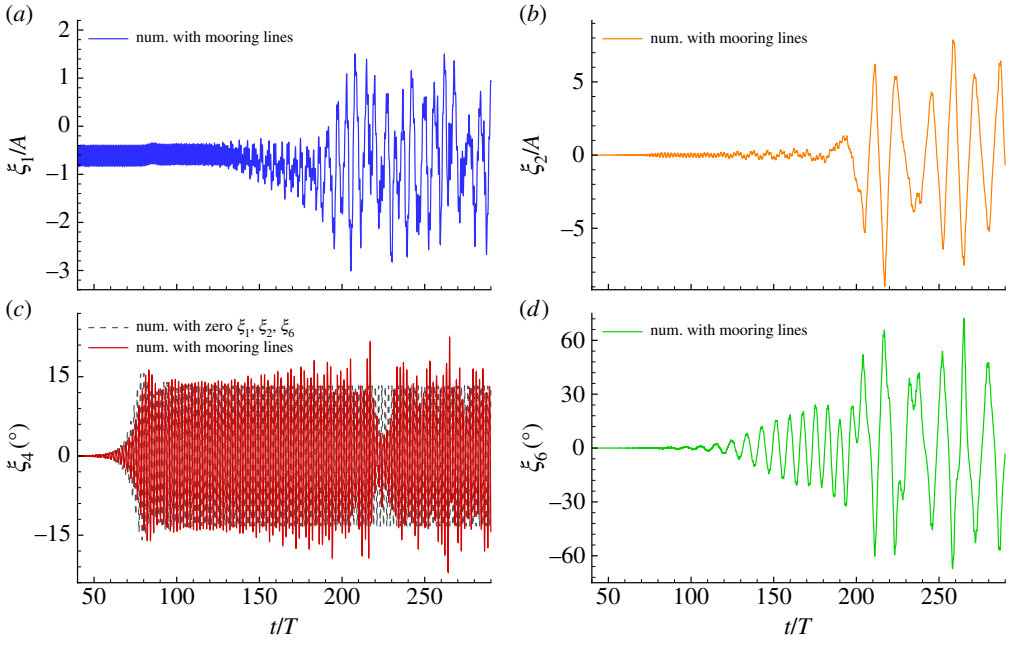

Figure 8. Incident waves with $\omega_{4n0}/\omega = 0.464$ and $kA = 0.15$: surge (*a*), pitch (*b*), roll (*c*) and yaw (*d*) motions. For the roll, the results from the simulation with zero surge, sway and yaw, is also given. (Online version in colour.)

Table 2. Occurrence of instability phenomena of the coupled system. NI, unstable on very long time scale or anyway with very limited motion amplitude; C, chaotic; NIC, with tendency to chaotic behaviour; B, breakdown of the simulation.

$\lambda/L \rightarrow$	0.75	1.00	1.25	1.50	2.00
$\omega_{4n0}/\omega \rightarrow$	0.402	0.464	0.519	0.568	0.656
method kA	instab.				
num moor 0.10	NI	yes/NIC	NI	NI	NI/C
num moor 0.15	yes	yes/C	yes/C	NI	yes
num moor 0.20	yes/C/B	yes/C	yes/C	yes/C	yes/C/B
num moor 0.25	yes/C/B	yes/C/B	yes/C	NI/C	yes/B

(c) Influence of motions coupling on the instability from weakly nonlinear solver

The influence of the individual motions on the occurrence and features of the unstable behaviour is examined for the same incident-wave case in figure 9 in terms of ξ_1, ξ_2, ξ_4 and ξ_6 at large times, i.e. $t > 300T$, through setting each of them separately to zero. Sway and yaw are the most important motions for instability occurrence, because by avoiding them no chaotic behaviour is induced, and only the roll is unstable owing to the parametric resonance caused by the ship interaction with the incident waves and by large heave and pitch motions. The surge and roll have a very limited effect on the amplitude level of the other motions, especially the latter, while the former tends to feed the chaotic regime occurrence. In addition, the earlier stages of the time evolution (not shown here) help in the investigation. The surge tends to delay the occurrence of the instability and affects also the beating frequency of the roll. The coupling with roll anticipates the occurrence of instability of yaw and sway.

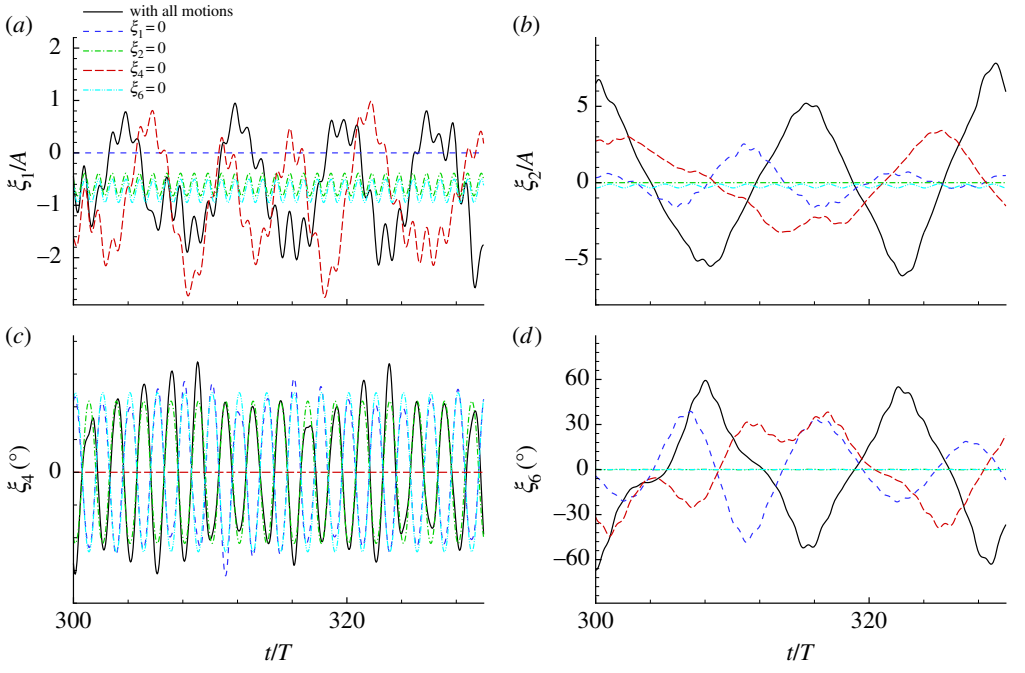

Figure 9. Incident waves with $\omega_{4n0}/\omega = 0.464$ and $kA = 0.15$: effect of motion coupling on the solution features at large times, i.e. at $t > 300T$. (*a*) Surge and (*b*) pitch. (*c*) Roll and (*d*) yaw. (Online version in colour.)

(d) Influence of motions coupling on the instability from a simplified stability analysis

In order to understand the behaviour of the moored ship in waves, a simplified stability analysis is also carried out. Because the major coupling is expected among sway, roll and yaw, the analysis has been limited to a 3 d.f. system, for which the motion equations

$$\sum_{j=2,4,6} (M_{ij} + A_{ij})\ddot{\xi}_j + B_{ij}\dot{\xi}_j + C_{ij}\xi_j = F_i(t) \quad i = 2, 4, 6 \tag{4.1}$$

hold when considering the ship as a linear system. By assuming a solution $\xi_i = \xi_{ia}\exp(st)$ for the ith degree of freedom, and setting the loads $F_i(t) = 0$, we obtain a linear equation system formally as $\mathcal{G}\,\boldsymbol{\xi}_a = 0$ for the motion amplitude vector $\boldsymbol{\xi}_a$. A non-trivial solution requires a zero determinant of the matrix, leading to the polynomial equation:

$$Hs^6 + Is^5 + Ls^4 + Ms^3 + Ns^2 + Ps + Q = 0 \tag{4.2}$$

whose solutions allow the investigation of the stability of the system. Because of the mooring system, the coefficients of the polynomial equation are, in general, different from zero. The damping coefficients owing to the cables are set as in the DD solver, so in the 3 d.f. system only $B_{22} = B^c_{22}$, B_{44} (from the hull) and $B_{66} = B^c_{66}$ are non-zero. Moreover, following Faltinsen [12] and from the adopted cable arrangement, the linear restoring coefficients provided by the cables are C^c_{22}, $C^c_{26} = C^c_{62} = C^c_{22} \cdot X_{\mathrm{moor}}$ and $C^c_{66} = C^c_{22} \cdot X^2_{\mathrm{moor}}$, whereas no linear restoring coefficients come from the hull for ξ_2 and ξ_6, meaning that $C_{ij} = C^c_{ij}$ for i and j equal to 2 or 6. So, for the examined cable arrangement, the coefficient

$$Q = C_{22}C_{44}C_{66} + C_{42}C_{64}C_{26} + C_{24}C_{46}C_{62} - C_{62}C_{44}C_{26} - C_{42}C_{24}C_{66} - C_{64}C_{46}C_{22}$$

is identically zero, i.e. $Q = C_{44}(C_{22}C_{66} - C_{62}C_{26}) = C_{44}((C_{22}X_{\mathrm{moor}})^2 - (C_{22}X_{\mathrm{moor}})^2) = 0$, leading to a null solution for s, whereas the other solutions are stable.

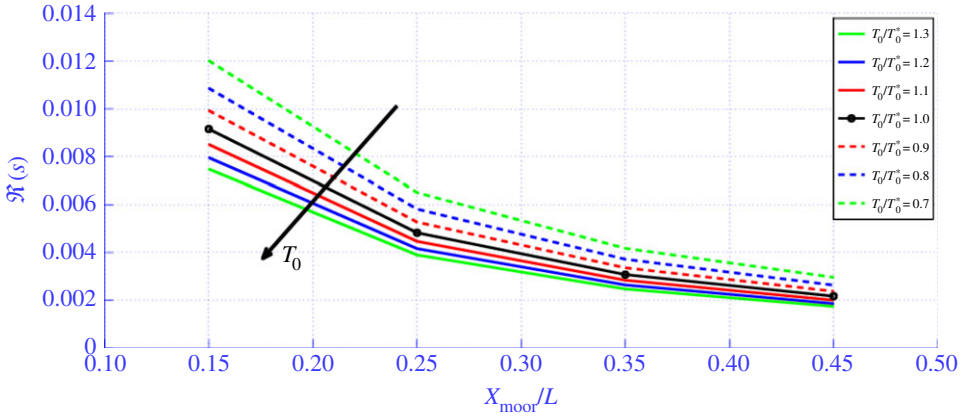

Figure 10. Stability analysis: real part of the sixth solution of equation (4.2) as function of the turret longitudinal position X_{moor} and for several values of the pre-tension. (Online version in colour.)

Table 3. Maximum amplitude of surge, sway, roll and yaw motions for $X_{moor} = 0.25$ and 0.4 and $\omega_{4n0}/\omega = 0.464$.

X_{moor}	kA	$\xi_{1,maxa}/A$	$\xi_{2,maxa}/A$	$\xi_{4,maxa}(^\circ)$	$\xi_{6,maxa}(^\circ)$
0.25	0.05	0.86	4.3×10^{-6}	1.2×10^{-6}	2.5×10^{-5}
0.40	0.05	0.86	6.3×10^{-6}	7.0×10^{-7}	1.5×10^{-5}
0.25	0.10	0.96	0.42	20.94	15.68
0.40	0.10	0.96	0.20	20.88	1.45
0.25	0.15	2.59	9.07	22.70	74.45
0.40	0.15	1.12	0.15	16.18	4.60

Actually, from the numerical simulations discussed above, the system should be unstable, suggesting an influence of nonlinear effects on the restoring coefficients and so on the stability. This was investigated using the weakly nonlinear solver to simulate forced sinusoidal motions in sway, roll and yaw separately, each at the uncoupled undamped natural frequency of the selected mode and with small amplitude (5 degrees for the angular motions and $0.01L$ for the sway). These simulations were used to identify equivalent linear restoring coefficients assuming the restoring loads in the form $F_i = C^n_{ij}\xi_j$. This provided C^n_{64}, C^n_{46}, C^n_{24} and C^n_{42} referred to as nonlinear motion-coupling coefficients in the following. In addition, the pre-tension for each cable was varied between 1400 and 2600 kN and X_{moor}/L between 0.15 and 0.45, so to perform a parameter investigation using reasonable values for FPSOs, also including $X^*_{moor} = 0.25L$ and $T^*_0 = 2000$ kN adopted in the present numerical studies.

Including C^n_{ij} in equation (4.2) and for all the values of X_{moor}/L and T_0, five s solutions are stable, whereas the sixth one is real and unstable and shown in figure 10. This means that the cables are not sufficient to avoid an unstable behaviour, though the instability appears on a quite long-time evolution as suggested by the limited values of $\mathcal{R}(s)$. By increasing the pre-tension and/or by moving the turret position forward, the value of $\mathcal{R}(s)$ decreases. This means that an optimal choice of the values of X_{moor} and T_0 cannot be identified within the geometric and tension practical limits.

To verify the trends from this simplified stability analysis, the 6 d.f. numerical solution for X^*_{moor} has been compared with the one for $X_{moor} = 0.4L$, using in both cases T^*_0 as pre-tension. The results are documented in table 3 in terms of maximum amplitude of surge, sway, roll and yaw motions for frequency ratio $\omega_{4n0}/\omega = 0.464$ and three different steepnesses. Consistent

Table 4. Stability analysis: real part of the sixth solution of equation (4.2) when all the nonlinear restoring coefficients listed in the table are set to zero (I) and when only C^n_{26} and C^n_{62} (II), or only C^n_{46} and C^n_{64} (III), or only C^n_{24} and C^n_{42} (IV), or all (V) are included (C^c_{26} and C^c_{62} are always different from zero in the analysis).

	C^n_{26}	C^n_{62}	C^n_{46}	C^n_{64}	C^n_{24}	C^n_{42}
I			0			
II	0.0081					
III			0.0041			
IV						0
V			0.0048			

with the stability analysis, for the lowest kA, no instability is recorded in both cases. Moreover, the weaker unstable behaviour for $X_{\mathrm{moor}} = 0.4L$ is confirmed by the results at the two higher steepnesses showing a much smaller amplitude for the horizontal motions. The roll amplitude remains of similar order of magnitude for the two X_{moor} because it is dominated by the PR owing to sufficiently large heave and pitch motions.

The importance of the coupling restoring terms $C_{ij} = C^n_{ij} + C^c_{ij}$, i.e. with $i \neq j$, and of the nonlinear coupling terms C^n_{ij} relative to the cable contributions C^c_{ij}, has been investigated through the simplified stability analysis. When all coupling terms are set to zero, the system is stable with three different complex solutions whose imaginary part is directly related with the corresponding resonance frequency of each degree of freedom. The same solutions are achieved for non-null C_{42}, C_{24} and/or C_{46} and C_{64}. The system becomes unstable only when C_{26} and C_{62} are set non-zero (independently from the presence of the other terms), and two of the three oscillatory solutions (identifiable in the yaw and sway motions) collapse in a single oscillatory solution. This confirms that the yaw–sway coupling is of major concern, causing the instability of the overall system.

In practice, owing to the cables, C^c_{26} and C^c_{62} are non-null, so a zero or unstable solution is expected. Table 4 reports the value of the unstable solution of equation (4.2), taking $C^c_{26} = C^c_{62}$ from the cables and examining the role of the nonlinear motion-coupling restoring coefficients with X^*_{moor} and T^*_{moor} as prescribed values for the turret position and pre-tension.

The first row refers to the case with all coupling terms C^n_{ij} set to zero and confirms a zero solution since $Q = 0$. The last row shows the case when all of them are considered, giving a positive value consistent with results in figure 10. The remaining rows examine the cases forcing to zero separately each couple of nonlinear motion-coupling coefficients showing that the main influence arises from the terms C^n_{26} and C^n_{62}. However, also the terms C^n_{46} and C^n_{64} play an important role.

(e) Influence of heading on the instability

The motion regimes, as well as their amplitudes at large times, i.e. at $t > 300T$, are influenced by the wave headings. This is examined in figure 11, still for the case with $\omega_{4n0}/\omega = 0.464$ and $kA = 0.15$ but with headings from 0 to 180°. Chaotic regime (indicated as C in the plots) for the motions occur in head- and bow-sea conditions. Going towards beam sea, the horizontal motions decay in time (D) and their oscillation amplitudes at large times become more limited and tend to be zero at 90°. As a consequence of this the roll is characterized by a steady-state (SS) behaviour. In quartering- and following-sea conditions, the horizontal motions show SS features and the SS behaviour of the roll is affected by an envelope (SSE) owing to the longer natural periods of the sway and yaw motions. The highest amplitudes of ξ_2, ξ_4 and ξ_6 occur in head and following seas while the surge is largest in quartering waves. The roll motion amplitude is less affected by the heading angle than those of the other motions. The incident-wave heading also matters for the mean values of the motions (figure 12). The yaw mean value increases from 0° to 180° when going from head- to following-sea conditions to rotate the platform towards the wave

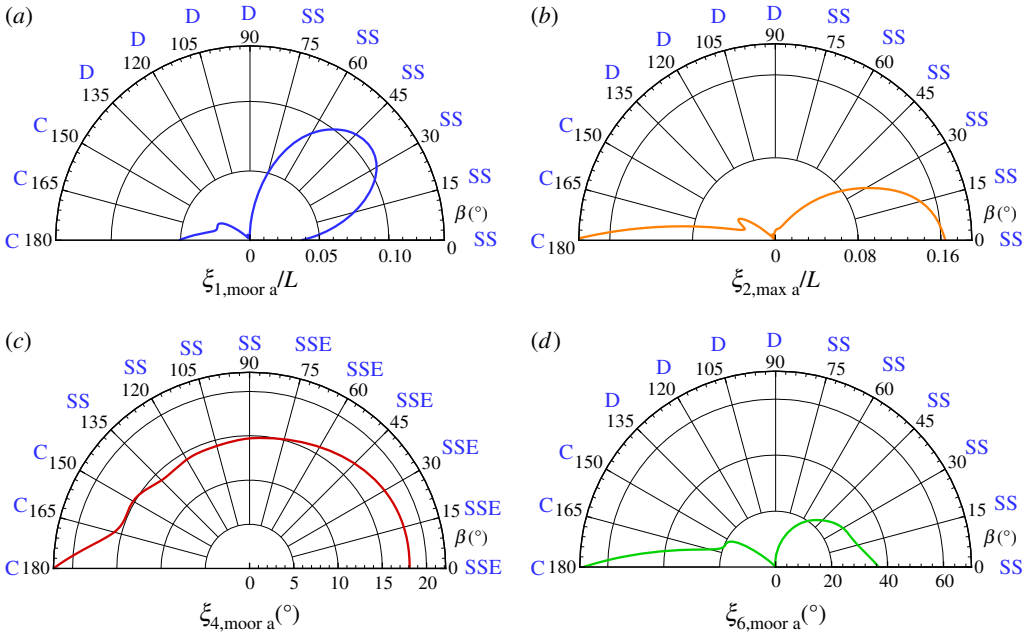

Figure 11. Incident waves with $\omega_{4n0}/\omega = 0.464$ and $kA = 0.15$ and heading from 0° to 180°: polar diagrams for the maximum amplitude of surge (*a*), sway (*b*), roll (*c*) and yaw (*d*) at large times, i.e. at $t > 300T$. The acronyms in the diagrams mean: C, chaotic; SS, steady-state; SSE, steady-state with envelope; D, decaying in time. (Online version in colour.)

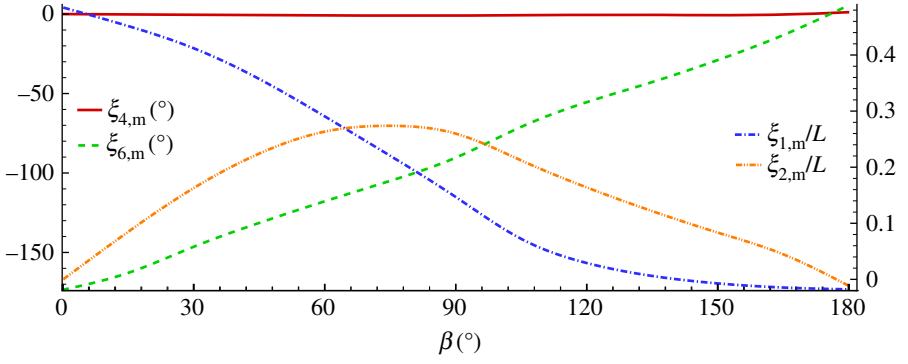

Figure 12. Incident waves with $\omega_{4n0}/\omega = 0.464$ and $kA = 0.15$: mean value of surge, sway, roll and yaw at large times, i.e. at $t > 300T$, for different heading conditions. (Online version in colour.)

direction and preserve a head-sea condition, consistently with the weather-vaning arrangement. Similarly, the surge mean value also increases, whereas the sway mean value has the maximum values towards beam-sea conditions. The recovery of head-sea conditions through the mooring-line systems explains why the roll amplitude is not much affected by the heading angle, and its mean value is also very limited and changes within ±1°.

(f) Influence of dynamic-positioning damping on the instability and cable tension

Because the mooring-line systems would not provide enough damping for large incident-wave steepness and frequency close to $\omega = \omega_{4n0}/0.464$, it is reasonable to combine them with thrusters. Figure 13 examines the effectiveness of a DP system in limiting the yaw and roll motions

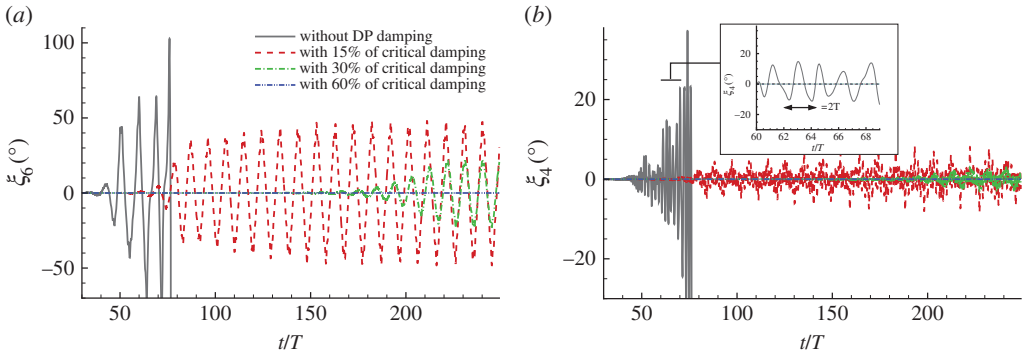

Figure 13. Incident waves with $\omega_{4n0}/\omega = 0.464$ and $kA = 0.25$: effect of damping from a dynamic positioning system on the (*a*) yaw and (*b*) roll motions. (Online version in colour.)

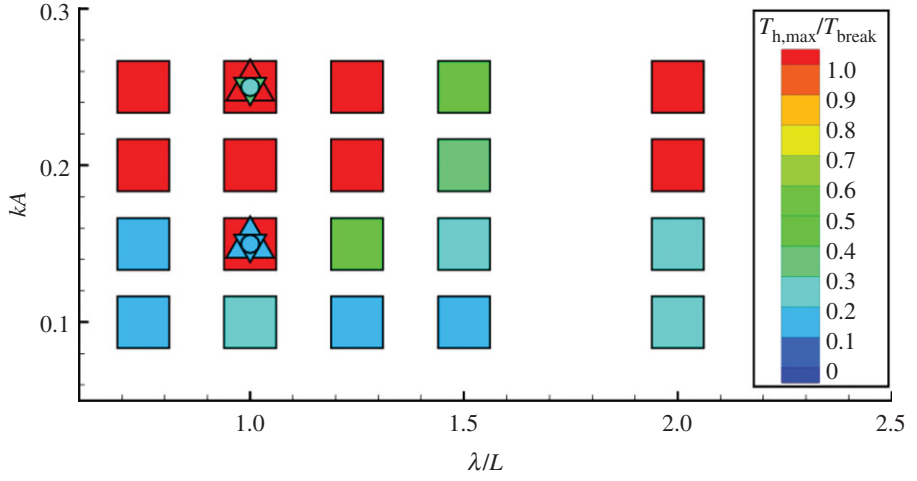

Figure 14. Maximum cable horizontal tension at the turret, T_{hmax}, as a function of the incident wavelength-to-ship length ratio and of the steepness. Squares: results without DP damping. Triangles: results with DP damping equal to the 15% of the critical damping. Gradients: results with DP damping equal to the 30% of the critical damping. Circles: results with DP damping equal to the 60% of the critical damping. The solutions with DP damping are estimated only for $\omega_{4n0}/\omega = 0.464$ with $kA = 0.15$ and with $kA = 0.25$. $T_{break} = 12\,000$ KN is taken as cable break tension. (Online version in colour.)

for the incident-wave case leading to the quickest breakdown of the simulations, i.e. with $\omega_{4n0}/\omega = 0.464$ and steepness $kA = 0.25$. It is assumed that the DP system can provide a linear damping equal to the 15%, 30% or 60% of the critical damping. For this incident-wave case, the sway–roll–yaw coupling is responsible for a PR resonance in the case of a pure mooring-line system (see the enlarged view in figure 13*b*). The PR is avoided by a DP giving 30% of the critical damping, whereas, among the three damping conditions, only 60% of the critical damping is suitable to control the yaw. One must note that the PR phenomena induced by the large heave and pitch motions are not avoided by the use of a DP system unless set to provide damping also for the vertical motions.

In terms of cable tension, for this incident-wave case, the 30% of the critical damping reduces T_h below the break load level, whereas the 15% of the critical damping is enough to avoid the cable failure for the case with $\omega_{4n0}/\omega = 0.464$ and $kA = 0.15$ examined above. This is shown in figure 14, also providing the results for a pure mooring-line system (square-coloured symbols). In the latter case, the failure is likely to occur near the first-parametric resonance and for waves sufficiently steep.

5. Conclusion

A three-dimensional numerical hybrid potential-flow seakeeping solver, based on the weak-scatterer theory for the external water–body interactions, on a shallow-water approximation for the water shipped on the deck and handling possible bottom-slamming occurrence with a local impact solution, has been extended to model the mooring-line loads. The latter are estimated assuming a nonlinear quasi-static approach requiring an iterative strategy to obtain the cable tension at the instantaneous cable configuration. The resulting solver was applied to investigate occurrence and features of PR on a weather-vaning FPSO with a turret single-point mooring-line system. The emphasis is given to the relevance of motions coupling and nonlinear effects on this phenomenon and on more general instability phenomena, as well as on the occurrence and severity of WOD. A parameter investigation has been carried out in terms of incident wavelength, wave steepness, heading angle, location of the turret and pre-tension. In addition, a simplified stability analysis was performed. From the results, sway and yaw tend to bring the system into an unstable regime with chaotic features. Surge and roll have a limited influence and tend, respectively, to delay and facilitate the instability. The sway–roll–yaw coupling widens the existence region of PR resonance and increases the PR severity for those events also occurring without mooring-lines. Moreover, it tends to cause larger amounts of shipped water, especially at smaller wavelength-to-ship length ratio and larger steepness. The chaotic features appear to be excited when a sufficiently large yaw amplitude is reached, suggesting an important role of nonlinear effects for the stability regime. This is confirmed by a simplified stability analysis showing the relevance of nonlinear restoring coefficients. More in detail, the coefficients connected with sway–yaw coupling are the most important and tend to destabilize the system. Then, we have the restoring coefficients associated with the roll–yaw coupling also becoming destabilized, whereas those connected with sway–roll coupling have a very limited effect. From the stability analysis, the system is always unstable for all longitudinal locations of the turret and for all pre-tensions examined; the instability weakens as the turret is moved forward and as the pre-tension is increased. The use of a suitable dynamic-positioning system can control the horizontal motions avoiding the instability and limiting the tension on the mooring, but it cannot avoid PR events induced by large heave and pitch motions unless set to provide damping also for the vertical motions.

Acknowledgement. The authors thank deeply Dr Skjørdal for providing relevant information of mooring-line arrangements used for FPSOs and related modelling.

Funding statement. This research activity is partially funded by the Research Council of Norway through the Centres of Excellence funding scheme AMOS, project number 223254, and partially by the Flagship Project RITMARE-The Italian Research for the Sea-coordinated by the Italian National Research Council and funded by the Italian Ministry of Education, University and Research within the National Research Programme 2011–2013.

References

1. Paulling JR. 2011 Parametric rolling of ships: then and now. In *Contemporary ideas on ship stability and capsizing in waves* (eds MAS Neves, VL Belenky, JO de Kat, K Spyrou, N Umeda). pp. 347–360. Amsterdam, The Netherlands: Springer.
2. Neves MAS, Rodríguez CA. 2011 On the assessment of coupled parametric rolling of ships in head sea. In *Marine technology and engineering: CENTEC anniversary book* (eds CG Soares, Y Garbatov, N Fonseca, AP Texeira), vol. 1, pp. 563–573. Lisbon, Portugal: Technical University of Lisbon.
3. Faltinsen OM. 2014 *Hydrodynamics of high-speed marine vehicles*. Cambridge, UK: Cambridge University Press.
4. Greco M, Lugni C, Faltinsen OM. 2014 Roll–yaw coupling effects on parametric resonance for a ship in regular waves. In *Proc. 29th Int. Workshop of Water Waves and Floating Bodies*, pp. 4. Osaka, Japan: Osaka University.

5. Greco M, Lugni C. 2012 3-D seakeeping analysis with water on deck and slamming. Part 1: numerical solver. *J. Fluids Struct.* **33**, 127–147. (doi:10.1016/j.jfluidstructs.2012.04.005)
6. Greco M, Colicchio G, Faltinsen OM. 2007 Shipping of water on a two-dimensional structure. Part 2. *J. Fluid Mech.* **581**, 371–399. (doi:10.1017/S002211200700568X)
7. Colicchio G. 2004 Violent disturbance and fragmentation of free surfaces. PhD thesis. University of Southampton, Southampton, UK.
8. Wagner H. 1932 Uber stoss- und gleitvorgange an der oberflache von flussigkeiten. *ZAMM* **12**, 192–235. (doi:10.1002/zamm.19320120402)
9. Pawlowski JS. 1991 A theoretical and numerical model of ship motions in heavy seas. *SNAME Trans.* **99**, 319–315.
10. Greco M, Lugni C, Faltinsen OM. 2014 Can the water on deck influence the parametric roll of a FPSO? A numerical and experimental investigation. *Eur. J. Mech. B/Fluids* **47**, 188–201. (doi:10.1016/j.euromechflu.2014.01.009)
11. Greco M, Bouscasse B, Lugni C. 2012 3-D seakeeping analysis with water on deck and slamming. Part 2: experiments and physical investigation. *J. Fluids Struct.* **33**, 148–179. (doi:10.1016/j.jfluidstructs.2012.05.009)
12. Faltinsen OM. 1990 *Sea loads on ships and offshore structures*. Cambridge, UK: Cambridge University Press.
13. Garza Rios LO, Bernitsas MM, Nishimoto K. 1997 Catenary mooring lines with nonlinear drag and touchdown. *Naval Archit. Mar. Eng.* (*SNAME*) **333**.
14. Cummins WE. 1962 The impulse response function and ship motions. In *Symp. on Ship Theory, Schiffstechnik*, vol. 9, pp. 101–109. Hamburg, Germany: Institut für Schiffbau der Universität Hamburg.
15. Offshore standard Det Norske Veritas. 2010 DNV-OS-E301 Position mooring. October 2010. Det Noske Veritas.